Pharm Res (2015) 32:3636–3648
DOI 10.1007/s11095-015-1722-2

RESEARCH PAPER

Structural Characterisation of Non-Deamidated Acidic Variants of *Erwinia chrysanthemi* L-asparaginase Using Small-Angle X-ray Scattering and Ion-Mobility Mass Spectrometry

David Gervais[1] • Darryl King[1] • Patrick Kanda[1] • Nicholas Foote[1] • Lucy Elliott[1] • Phillip Brown[1] • Natacha O. Lee[2] • Konstantinos Thalassinos[2] • Claire Pizzey[3] • Robert Rambo[3] • Thomas C. Minshull[4] • Mark J. Dickman[4] • Stuart Smith[1]

Received: 23 March 2015 / Accepted: 20 May 2015 / Published online: 4 June 2015

ABSTRACT

Purpose *Erwinia chrysanthemi* L-asparaginase (ErA) is an enzyme commonly used in the treatment regimen for Acute Lymphoblastic Leukaemia (ALL). Biopharmaceutical products such as ErA must be monitored for modifications such as deamidation, typically using ion-exchange chromatography (IEX). Analysis of clinical-grade ErA using native IEX resolves a number of enzymatically-active, acidic variants that were poorly characterised.

Methods ErA IEX variants were isolated and fully characterised using capillary electrophoresis (cIEF), LC-MS and LC-MS/MS of proteolytic digests, and structural techniques including circular dichroism, small-angle X-ray scattering (SAXS) and ion-mobility mass spectrometry (IM-MS).

Results LC-MS, MS/MS and cIEF demonstrated that all ErA isolates consist mainly of enzyme lacking primary-sequence modifications (such as deamidation). Both SAXS and IM-MS revealed a different conformational state in the most prominent acidic IEX peak. However, SAXS data also suggested conformational differences between the main peak and major acidic variant were minor, based on comparisons with crystal structures.

Conclusions IEX data for biopharmaceuticals such as ErA should be thoroughly characterised, as the most common modifications, such as deamidation, may be absent.

KEY WORDS deamidation · ion mobility · L-asparaginase · pH-induced conformational change · SAXS

ABBREVIATIONS

AHA	L-aspartic acid-β-hydroxamate
ALL	Acute Lymphoblastic Leukaemia
CCS	Collision Cross Section
CD	Circular Dichroism
CID	Collision-Induced Dissociation
cIEF	Capillary Isoelectric Focussing
DP	Drug Product
DS	Drug Substance
EcA	*Escherichia coli* L-asparaginase
ErA	*Erwinia chrysanthemi* L-asparaginase
ESI	Electrospray Ionisation
HPLC	High-Pressure Liquid Chromatography
I(q)	Scattering Intensity
IEX	Ion-Exchange Chromatography
IM-MS	Ion Mobility-Mass Spectrometry
LC-MS	Liquid Chromatography-Mass Spectrometry
LC-MS/MS	Liquid Chromatography-Tandem Mass Spectrometry
MES	2-(N-morpholino)ethanesulfonic acid
MS	Mass Spectrometry
MWCO	Molecular Weight Cut-Off
P(r)	Pair-Distance Distribution Function
PBP	Pheromone-Binding Protein
PDB	Protein Data Bank

Electronic supplementary material The online version of this article (doi:10.1007/s11095-015-1722-2) contains supplementary material, which is available to authorized users.

✉ David Gervais
dave.gervais@portonbiopharma.com

[1] Porton Biopharma Limited, Porton Down, Salisbury, Wiltshire SP4 0JG, UK

[2] Institute of Structural and Molecular Biology, Division of Biosciences, Darwin Building Room 101A, University College London, Gower Street, London WC1E 6BT, UK

[3] Diamond Light Source Ltd., Harwell Science and Innovation Campus, Didcot, Oxfordshire OX11 0DE, UK

[4] ChELSI Institute, Dept of Chemical and Biological Engineering, University of Sheffield, Mappin Street, Sheffield S1 3JD, UK

PTM	Post-Translational Modification
q	Scattering Vector
R_g	Radius of Gyration
SAXS	Small-Angle X-ray Scattering
SDS-PAGE	Sodium Dodecyl Sulphate Polyacrylamide Gel Electrophoresis
TOF	Time-of-Flight
UPLC	Ultra High Pressure Liquid Chromatography
V_c	Volume of Correlation
WT	Wild-Type
XIC	Extracting Ion Current

INTRODUCTION

The enzyme L-asparaginase (EC 3.5.1.1) catalyses the production of free aspartic acid (Asp) using the substrate asparagine (Asn). L-asparaginase is produced commercially from two organisms, *Erwinia chrysanthemi* (ErA) and *Escherichia coli* (EcA) (1), and both enzymes (ErA and EcA) are used clinically in the treatment of acute lymphoblastic leukaemia (ALL) (2, 3). ErA is marketed as Erwinase® or Erwinaze® (4) and is an important part of the overall ALL treatment regimen. As ErA is immunologically distinct from EcA, patients who develop hypersensitivity reactions to EcA may often be successfully treated after a switch to ErA.

The enzyme ErA exists as a 140 kDa homotetramer in its active form. The native tetramer has an apparent isoelectric point of pH 8.6 (5), and the inactive 35 kDa subunit consists of 327 amino acids. The crystal structure of the enzyme has been previously determined to 1.8 Å resolution (6–8) and the active site is known to involve a number of residues, including Thr15, Ser62, Glu63, Thr95, Asp96, and Ala120 (6). Recently, the manufacturing process for ErA has been investigated and validated using modern analytical techniques (9).

Biopharmaceutical manufacturing processes, such as that for ErA, can have an impact on the amount of product-related variants in the final clinical material (10). These product-related variants, often present in only minor quantities, may include forms carrying post-translational covalent modifications (PTM) such as deamidation or methionine oxidation, or may reflect the presence of protein-protein aggregation (11). Understanding and controlling the amounts of these product-related variants is a major challenge in the development and manufacture of biopharmaceutical products. In particular, protein deamidation is a common process-induced PTM (10, 12, 13).

Analysis and quantitation of deamidation in proteins is typically achieved using ion-exchange HPLC (IEX) (14), capillary electrophoresis (15) or liquid chromatography-mass spectrometry (LC-MS) techniques (16). However, deamidation can sometimes be artefactually induced by extreme pH conditions during proteolytic digestion prior to LC-MS (17), making quantitative MS analyses difficult. Typically in routine samples during biopharmaceutical development and manufacture, IEX (18, 19) or capillary isoelectric focussing (20, 21) are used for quantification of acidic variants including deamidated species. For IEX in particular, it can be difficult and time-consuming to ascertain what PTMs are present in the various acidic and basic peaks (22, 23). IEX is used routinely in the analysis of ErA manufacturing samples (24) and a relationship between the time used for thawing cells and IEX results was established.

Recently, deamidation in ErA has been studied in detail, including characterisation of recombinant deamidated ErA mutants (25) and development of a fully denaturing cIEF method for quantitation of deamidation in ErA samples (26). Using cIEF, acidic species (including deamidation) were found to be very low in routine ErA samples. However, the extent of acidic species in ErA manufacturing samples (1.5–4.0% by cIEF) was lower than the typical numbers obtained using IEX (8–15%). Based on this lack of agreement between the two techniques, there was an unanswered question about what the IEX acidic species represented, apart from deamidation. The aim of the present work was to isolate the ErA acidic-variant peaks using IEX, and fully characterise them using a variety of analytical and structural techniques.

MATERIALS AND METHODS

All reagents were from Sigma (Dorset, UK) unless otherwise indicated.

Source of Enzyme

Samples of ErA Drug Substance (DS) for fractionation were provided by Porton Biopharma Limited, Porton Down, UK. The composition of ErA DS is approximately 45 mg/mL protein in 10 mM sodium chloride. The DS is stored at −20°C and upon thawing, the typical pH of the protein solution is 7.8–8.4. ErA DS is later formulated and lyophilised to generate the final Drug Product (DP) form, consisting of (nominal) 10 mg protein per vial with 0.5 mg sodium chloride and 5 mg glucose monohydrate.

Generation of IEX Peak Isolates

Samples of the isolated IEX peaks C, D and F were generated as follows. Frozen (−20°C) aliquots of purified ErA drug substance (DS) were used as the starting material. A semi-preparative WCX-10 column (Dionex, Leeds, UK) with dimensions 9 × 250 mm, was used for the isolation with a Waters HPLC workstation (Elstree, UK). The mobile phase consisted of two buffers: buffer A was 10 mM sodium chloride in 20 mM sodium phosphate pH6.2, and buffer B was

300 mM sodium chloride in 20 mM sodium phosphate pH 6.2. The flow rate through the column was 3 mL/min using a gradient (Table I), and the absorbance was monitored at 220 nm. Multiple chromatographic cycles were used, with 4 mg protein injected per cycle. Peaks were collected manually during each cycle into glass Duran bottles. During the repeat cycles, peaks were kept segregated on ice at 2–8°C, and concurrently concentrated using Millipore (Watford, UK) Amicon Ultra-15 regenerated cellulose 10 kDa MWCO spin concentrators.

When the total volumes of the three peak isolates from all chromatographic cycles (C, D and F) had been reduced to approximately 1000 µL, they were analysed for protein concentration using absorbance at 280 nm, and desalted into 10 mM sodium phosphate pH 7.2 using NAP-10 columns (GE Healthcare, Amersham, UK). The volume needed to achieve 5 mg/mL protein concentration was calculated for each desalted isolate, and the concentration was continued in Ultra-4 regenerated cellulose 10 kDa spin concentrators. The volumes of the final 5 mg/mL concentrates were carefully measured and topped up with 10 mM sodium phosphate pH 7.2 if required, to accurately achieve the desired 5 mg/mL concentration. Samples were aliquoted into 50 µL portions (250 µg protein per aliquot) and frozen at −20°C until further analysis.

Analytical IEX

Samples of the isolated peaks C, D and F were analysed using the previously-described IEX method (24) to ensure that they were enriched in the peak of interest. The IEX buffers were prepared as described for preparative IEX above. Samples were also analysed pre- and post-refolding experiments. Analytical traces were integrated using Empower 2 (Waters, Elstree, UK).

Capillary Isoelectric Focussing (cIEF)

The cIEF analyses were conducted according to the N-ethylurea-urea method described previously (26). Briefly, a master mix was prepared containing 8 M urea, 2.2 M N-ethylurea, 0.35% methylcellulose (ProteinSimple, Toronto, Canada), and 4% Pharmalytes 3–10. A 200 µL aliquot of master mix was combined with 1 µL of low-p*I* marker (5.85) and 1 µL of high-p*I* marker (9.5) and protein sample was added to a final target concentration of between 0.1 and 0.2 mg/mL. Samples were vortexed to ensure proper mixing, spun briefly at 13,000 rpm in an Eppendorf table-top centrifuge to remove air bubbles, and injected into a iCE3 instrument (ProteinSimple) with FC cartridge. Samples were focussed at 1.5 kV for 1 and 12–13 min at 3 kV, and the resulting data traces were integrated using Empower 2 with Savitsky-Golay smoothing.

Table I Gradient Table for Semi-Preparative IEX

Time (min)	Flow (mL/min)	%A	%B
0	3	93	7
4	3	93	7
24	3	84.8	15.2
26	3	0	100
28	3	93	7
30	3	93	7

Circular Dichroism (CD) Analyses

Circular Dichroism analyses of the IEX peak isolates were conducted using a Jasco J-715 spectropolarimeter at Alta Bioscience (Birmingham, UK). Samples were shipped on dry ice and held frozen at −20°C until the time of analysis. The analyses were carried out between 190 and 280 nm, and appropriate blank buffers (10 mM sodium phosphate pH 7.2) were provided for the analysis.

Asparaginase Activity Assay

The asparaginase activity of ErA samples was determined using the UV Activity assay as described previously (27). Briefly, the assay was performed in borate buffer in the presence of substrate by measuring the change in the amide bond absorption at 225 nm. As L-asparagine is depleted in the sample, the UV absorbance decreases and the slope of the absorbance curve is compared to a standard ErA sample with known activity.

K_m and k_{cat} Determination

The Michaelis constant (K_m) and catalytic constant (k_{cat}) of the ErA IEX isolates was determined using the substrate L-aspartic acid-β-hydroxamate (AHA) as described previously (28).

Small-Angle X-ray Scattering

The ErA IEX Isolates for Peaks D and F only were analysed using static Small-Angle X-ray Scattering (SAXS). The SAXS experiments were conducted at Diamond Light Source (Didcot, UK). Samples were centrifuged for 10 min at 10°C prior to analysis. The samples were loaded onto a 96-well plate for measurement, with each well containing approximately 25 µL of solution. SAXS data were collected at 15°C on beamline B21 using 12.4 keV X-rays and a Pilatus (Dectris, Switzerland) 2 M area detector. Data were collected as a series of 30 frames of 10 s duration. Data reduction was performed

in a standard manner using software developed at Diamond and data analysis was performed using the software ScÅtter (www.bioisis.net). For background (buffer) measurements, all 30 frames were averaged. The SAXS from the background (buffer) was subtracted from the corresponding protein SAXS measurement. Protein datasets were inspected for radiation damage and none was observed in any dataset. No aggregation was detected in any of the protein datasets, so all 30 frames were averaged.

LC-MS of Double-Digests

Samples were co-digested with two proteolytic enzymes and analysed using UPLC- TOF-MS. For the digestion, 250 µg of each peak isolate was first denatured with RapiGest™ detergent (Waters, Elstree, UK) for 20 min at 65°C. The samples were then incubated at 37°C with Glu-C protease (Promega, Southampton, UK) at 1:25 w/w enzyme:substrate ratio for 22 h, followed by addition of trypsin (Promega) again at 1:25 w/w enzyme:substrate ratio for 3 h. The digest reactions were stopped with the addition of an equal volume of 6 M Guanidine HCl, filtered, and analysed. The UPLC column was a Waters (Elstree, UK) Acquity BEH C_{18} with dimension 2.1×150 mm and 1.7 µm particle size. The flowrate was 0.4 ml/min, column temp was at 60°C, and the mobile phase consisted of a 0–42% gradient of 0.1% TFA/acetonitrile (Solvent B) in Solvent A (0.1% TFA/H_2O) over 60 min. The effluent was monitored at 220 nm, and the detector was interfaced with a Waters LCT Premiere Time of Flight (TOF) mass spectrometer, which had been calibrated with a sodium iodide-cesium iodide solution in the 100–4000 mu range. Mass spectrometer settings included a capillary voltage of 3200 V, cone voltage of 25 V, and N_2 desolvation flow at 900 l tr/h at 350°C. M/z was monitored between 100 and 4000 mu using MassLynx (Waters) software, and masses were corrected by periodic sampling of a leucine-enkephalin reference solution (LockSpray™) during data acquisition. The resulting TIC chromatogram was processed by Waters BiopharmaLynx software™ and the results tabulated based on the predicted fragmentation profile from the GluC/Trypsin substrate specificities, including standard possible covalent modifications (oxidation, deamidation, etc.) and expected salt/solvent adducts of intact fragments.

LC-MS/MS of Double-Digests

GluC-Trypsin digests were also analysed using LC-MS/MS. Digests were prepared as described above, and split in half. The first portion of the material was analysed as described for LC-MS above. The second half of the material was analysed as follows. A 2 µg portion of each sample was buffer exchanged into MS compatible buffers using HyperCarb tips (ThermoFisher, Hemel Hempstead, UK) according to supplied protocol (to remove 3 M Guanidine Hydrochloride). Following this, samples were dried and resuspended in 10 µl of 0.1% TFA (LC-MS grade) and 5 µl was analysed using MS analysis.

The MaXis Ultra high resolution quadrupole time-of-flight (Q-ToF) system (Bruker Daltonics, Coventry, UK) with an online UltiMate 3000 RSLCnano HPLC (ThermoFisher) was used to acquire spectra. Collision Induced Dissociation (CID) was used to generate MS/MS spectra. A 150 mm× 75 µm ID PepMap reversed phase column (ThermoFisher) was used. Data were acquired over 79 min using the gradient listed in Table II. Buffer A was 0.1% formic acid (FA) and 3% acetonitrile (ACN) (LC-MS grade), and Buffer B was 0.1% FA, 97% ACN. MS and MS/MS scans (m/z 50–2000) were acquired in positive ion mode. Lock mass calibration was performed using HP 1221.990364. Line spectra data were then processed into peak list by Data Analysis (Bruker Daltonics) using the following settings. The sum peak finder algorithm was used for peak detection using a signal to noise (S/N) ratio of 10, a relative-to-base peak intensity of 0.1% and an absolute intensity threshold of 100.

Data were analysed in Data Analysis software (Bruker Daltonics) and used to create .mgf files. The .mgf files were then searched in MASCOT using Mascot Daemon (Matrix Science, Boston, USA). MS and MS/MS tolerance were set at 0.15 Da, and searched against the SwissProt database with the Eubacteria Taxonomy selected. Variable modifications selected were Oxidation (M), Deamidation (NQR) and Gln->Pyro-glu conversion (N-term). Enzymes selected were Glu-C + trypsin, with 5 missed cleavages allowed. Charge states searched were 2+, 3+ and 4+. A peptide ion score of ≤10 as a cut-off as calculated by Mascot was also used to filter the results. High resolution extracted ion chromatograms (hXIC) were generated in DataAnalysis (Bruker Daltonics) for comparative quantification of peptides.

Sodium Dodecyl Sulphate Polyacrylamide Gel Electrophoresis (SDS-PAGE)

Samples were run on SDS-PAGE using Invitrogen (Paisley, UK) Novex™ pre-cast NuPage (Invitrogen) 4–12% Bis-Tris

Table II LC-MS/MS Gradient Details

%B	Time (min)	Flow rate (µl/min)
4	0–5	0.3
4–40	5–60	0.3
40–90	60–61.1	0.3
90	61.1–67	0.3
90–4	67–68.1	0.3
4	79	0.3

gels, 1.0 mm. Samples were diluted to 0.1 μg/mL protein using NuPage 4x sample buffer, NuPage 10x reducing agent and water, and heated at 70°C for 10 min. A sample loading of 10 μL per well (1 μg per well) was used for the protein samples. Gels were run using MES running buffers and electrophoresed at 200 V constant voltage for 35 min, and stained using Invitrogen SafeStain before imaging using a Bio-Rad (Hemel Hempstead, UK) GS-800 densitometer.

Ion Mobility Mass Spectrometry

Prior to mass spectrometry analysis all samples were buffer exchanged five times into 200 mM Ammonium acetate. Samples were then diluted to 5 μM and either infused into the mass spectrometer using borosilicate capillaries prepared in-house, or further buffer exchanged into denaturing solvent (50% acetonitrile, 0.1% formic acid) using ZipTip pipette tips (Merck, UK). All samples were analysed using a Synapt HDMS mass spectrometer (29) (Waters, UK). Instrument tuning parameters for denaturing conditions were: capillary voltage 1.2 kV, source temperature 40°C, Trap 6.0 V, Transfer 4.0 V. For native and ion mobility analyses instrument tuning parameters were: capillary voltage 1.2 kV, source temperature 40°C, Trap 8.0 V, Transfer 6.0 V, Bias 20 V, TWave velocity 285 m/s, TWave height 11 V, IMS gas pressure 0.52 mbar and backing pressure 4.8 mbar.

Mass spectrometry data were processed using MassLynx (Waters, UK). Arrival time distributions were converted to collision cross sections (CCS) by calibrating against known CCS values from the standard proteins ConA, BSA and β-lactoglobulin. CCS calibration was performed using Amphitrite (30).

RESULTS AND DISCUSSION

Ion-exchange chromatography (IEX) is a technique routinely used in the study of protein samples, and in particular to assess the presence of charge-variant species during biopharmaceutical development and manufacture. Many separations are now conducted using HPLC columns with polymeric, nonporous, chromatographic media that have grafted ion-exchange functionalities (14). Such media are designed to eliminate competing retentive elements from the analysis, leaving ion-exchange as the dominant separation mechanism. During these kinds of analyses it is usually reasonable to assume, therefore, that size-based differences in chromatographic peaks are negligible and that any separation observed is due to differences in protein charge.

In a typical IEX analysis of purified ErA from manufacture (Fig. 1), a reproducible peak signature is observed. The method is run under native, non-denaturing conditions and therefore the peaks that elute are a representation of the different

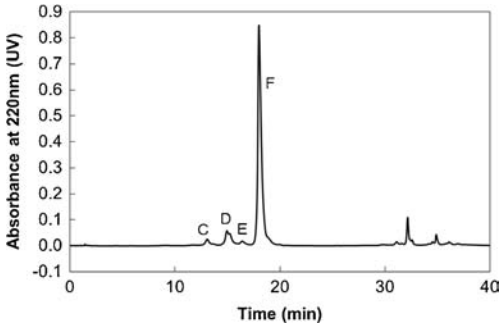

Fig. 1 Typical purified ErA IEX chromatographic profile. The peaks of interest are labelled (**c**, **d**, **e** and **f**).

ErA charge variants present in the original sample. A number of acidic peaks (or acidic species) elute prior to the main band. These acidic species, labelled for convenience as Peaks C, D and E, have an apparently lower isoelectric point (pI) compared to the main product peak, labelled Peak F. Using SE-HPLC, ErA peaks C, D and F were shown to consist solely of unaggregated enzyme (data not shown). The peaks eluting later than Peak F in the IEX assay are known to be due to the presence of protein-protein aggregates and were not investigated further in this work. Understanding the nature of the acidic species peaks, in particular C and D, compared with Peak F, was the main focus of this work. It should be noted that Peak E, due to its close proximity to the very large component Peak F, could not be isolated and therefore was not studied in detail. During semi-preparative chromatography, in order to avoid contamination of the Peak F isolate with Peak E, collection of Peak F only started several minutes after its first appearance (but while the UV signal in the detector was still saturated, indicating F was continuing to elute).

Deamidation is one of the most common PTMs giving rise to charge heterogeneity in bacterial, non-glycosylated proteins. The effects of deamidation at selected sites in ErA has been studied previously (25) and was demonstrated not to negatively impact the enzyme activity or kinetic properties. A denaturing capillary isoelectric focussing (cIEF) technique (26) was developed using ErA and deamidated variants as model proteins. Using this cIEF method, purified ErA samples from manufacture were shown to have low levels (1.5–4.0%) of deamidated (low-pI) peaks. These levels of deamidation in ErA determined by cIEF were much lower than the typical acidic species content (UV absorbance at 220 nm) observed using IEX (8.0–15.0%). It was previously postulated that the IEX acidic species peaks C, D and E (24) represented deamidated ErA species. However, the lack of correlation between the two measures (IEX and cIEF, data not shown) suggested that the IEX acidic species may reflect a variety of modifications to ErA, of which deamidation was only a small component. Therefore, it was decided to isolate and study these IEX peaks in detail.

The ErA peaks C, D and F were isolated using semi-preparative chromatography, concentrated and desalted prior to analysis using IEX to ensure enrichment in the peak of interest. The analytical IEX chromatograms (Fig. 2) of these isolates demonstrated that the peaks C and D had been enriched from approximately 3 and 10% respectively in the parent material to ≥60% each in the isolated materials. The peak F isolate was found to be essentially free of other acidic species by IEX. For peak isolates of C and D, repeated attempts to further enrich the purity by IEX were unsuccessful, resulting in either near-total loss of enzyme or similar levels of IEX purity (data not shown). The reasons for the apparent contamination of C and D isolates with peak F material were unclear, but may be due to equilibrium between the different IEX species, or to a lack of resolution during semi-preparative isolation. It should be noted that the isolates maintained a consistent chromatographic profile when analysed by IEX, so any equilibrium effect did not alter the overall composition of the isolates. However, ErA is a tetrameric enzyme and multiple forms may be present within a single IEX peak. Due to these factors and considerations, it was decided to proceed to characterisation of these isolates.

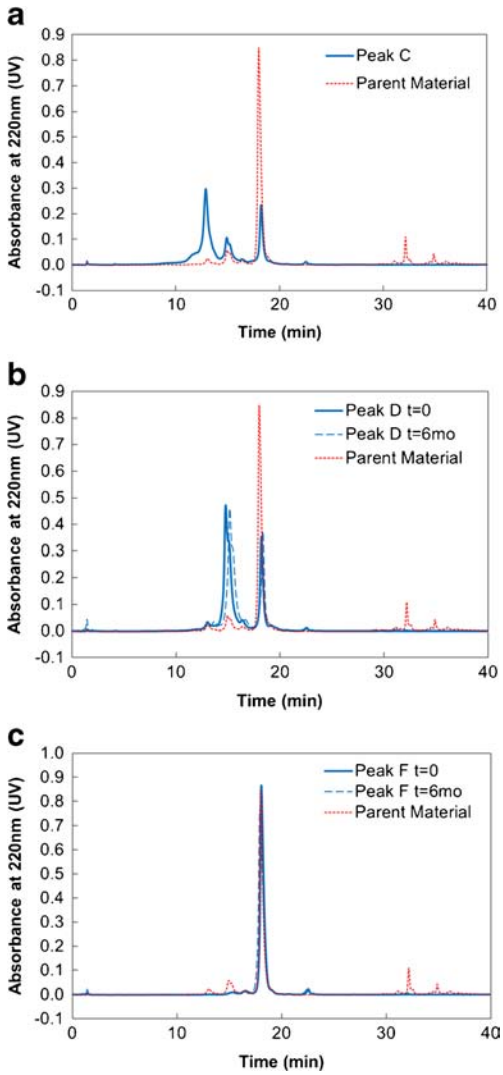

Fig. 2 Analytical IEX chromatograms for isolated semi-preparative IEX fractions. Each fraction is shown with an overlay of the parent ErA material used for isolation. The three fractions enriched in the various IEX peaks C (**a**), D (**b**) and F (**c**) are shown.

In order to illustrate the stability of the isolated fractions, the isolates D and F were measured using analytical IEX at both the time of isolation ($t=0$) and after 6 months long-term storage at −20°C (Fig. 2b and c), without significant change in the chromatographic profile. All of the analytical techniques employed to study these isolates were conducted during this 6 month time window. These data indicate that the composition of the isolates did not change during the storage period and illustrate the suitability of these isolates for the study.

The three isolates were found to compare well in terms of enzymatic activity (Table III) and electrophoretic mobility as measured by SDS-PAGE (Fig. 3). All three peak isolates appeared comparable to the reference material by SDS-PAGE. The peak isolates further compared well in terms of enzymatic constants (Table IV). The peak C isolate had a slightly lower k_{cat} compared to the peak D and F isolates, but reasons for this were not immediately apparent.

The three peak isolates were analysed using the denaturing cIEF in the presence of 8 M urea and 2.2 M N-ethylurea. The results (Fig. 4) demonstrated that in all three peaks, unmodified (p*I* 7.35) ErA was the main species (82, 93 and 100% in C, D and F isolates respectively), with several minor peaks representing modified ErA (putative deamidated species) present in Peak C and D isolates only. These results strongly suggested that the IEX acidic peaks C and D represent forms of ErA due to other changes, and not due to deamidation as previously believed. Mathematically, the levels of modified species measured by cIEF in Peaks C and D equate to roughly 1–1.5% in the parent material, which is in line with previously-determined levels of cIEF low-pI species in ErA (26).

The observed lack of putative deamidation in the IEX peak isolates C and D led to further investigation using LC-MS. Samples were digested using two proteolytic enzymes and analysed using reversed-phase LC and time-of-flight (TOF) MS. In all three samples analysed (IEX Peak isolates of C, D and the main peak F), no significant levels of deamidation were observed (see BiopharmaLynx-processed peak lists in

Table III Enzymatic Activity of IEX Peak Isolates

Sample	Activity (U/mL)	Protein A280 (mg/mL)	Specific activity (U/mg)
Fraction C	3726.1	5.0	745.2
Fraction D	3971.8	5.0	794.4
Fraction F	3762.5	5.0	752.5

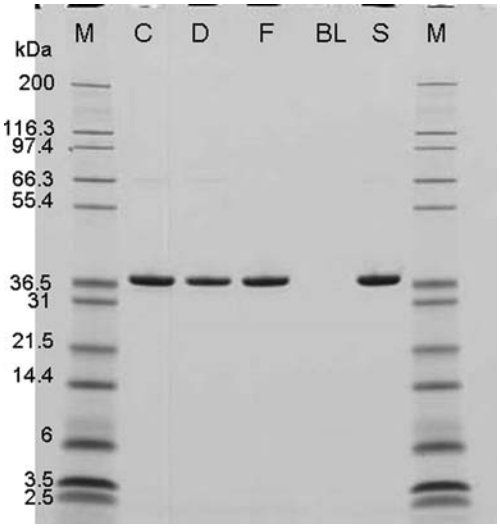

Fig. 3 SDS-PAGE analysis of isolated IEX peaks. The lanes in the gel correspond to the samples as follows: *M* Mark12 Standard, *C* Peak C, *D* Peak D, *F* Peak F, *BL* blank, *S* ErA reference material. The minor band at 66 kDa is likely to represent incomplete denaturation during SDS sample preparation.

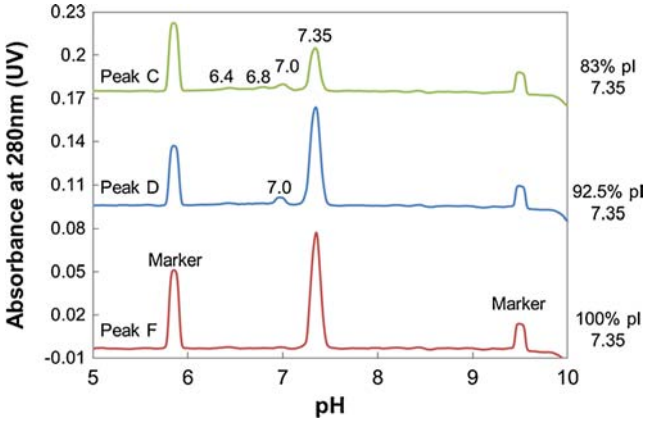

Fig. 4 Capillary isoelectric focussing of IEX peak isolates. The pI values corresponding to the various cIEF peaks are indicated in the figure. The main peak (pI 7.35) integration area percent, as determined using Empower 2, is shown on the right hand side of the figure.

Supplementary Tables). The only significant PTM that was observed by LC-MS (Table V) was methionine oxidation; however, the levels of oxidation were low and consistent between the three IEX Peak isolates (C, D and F) suggesting this was a method-induced artefact. Other PTMs not observed in these samples, but included in the LC-MS search criteria were hydroxylation (Lysine), formylation (Lys), carbamylation (Lys & Arg), and acetylation (Lys), all of which could have decreased the positive charge on the surface. One peptide (QFSNMASE) was observed to contain pyro-Glu at the N-terminus consistently in all isolates, but this was shown to be an artefact induced by the digestion procedure (data not shown). Critically, the levels of various PTMs observed in all IEX peak isolates were sub-stoichiometric, ruling out assignment of any of the IEX peaks as representing one change in isolation. A small amount of the succinimide (deamidation intermediate) was observed at the theoretically-labile residue N_{281}; however, the levels were consistent among all three peak isolates. This result is likely to be an assay artefact, due to exposure (25 h) of this residue to slightly basic conditions of the digestion procedure.

The results obtained using LC-MS were further confirmed with LC-MS/MS. As for the LC-MS results discussed above, LC-MS/MS only detected deamidation of low abundance compared to the unmodified peptide. Typical XIC chromatograms of a deamidated and non deamidated peptide identified in the LC MS/MS are shown in Fig. 5 (further information provided in Supplementary Information). Routinely, deamidated peptides are detected using ESI MS/MS, due to the high sensitivity of the instruments and the background chemical deamidation that occurs during sample preparation and sample analysis. The levels detected in the ErA IEX peak isolates were consistent with background deamidated peptides from typical proteomic experiments and analysis.

Taken together, the cIEF, LC-MS and LC-MS/MS data indicated that primary-structure modifications were not the primary cause for the separation of various IEX species. Therefore, it was decided to investigate higher-order structural and conformational influences on the IEX charge-based separation, with the rationale that slight changes in salt bridges or hydrogen bonding could cause apparent differences in p*I* (and therefore IEX retention time) in the native state. This rationale was further supported by refolding experiments (Fig. 6) conducted with the peak isolate samples. Peaks were exposed to a mixture known for efficiency of denaturation with ErA samples (8 M urea with added 2.2 M N-ethylurea) (26) before renaturation by dialysis into 18.2 MΩ water and analysis using IEX. The results of these experiments demonstrated that isolated

Table IV K_m and k_{cat} Data for IEX Peak Isolates

Sample	K_m (μM)	K_m 95% confidence interval (μM)	k_{cat} (s^{-1})	k_{cat} 95% confidence interval (s^{-1})
Fraction C	256	244–269	420	411–429
Fraction D	265	250–281	512	499–525
Fraction F	259	241–276	503	489–518

Table V LC-MS Significant Modifications in ErA Peak Isolates from IEX. Differences in Modifications Seen in GluC/Trp Digests of P125 WCX Peaks C, D and F. Data are Expressed as the Fraction (percent) of Parent ion Intensities. Proteolytic Fragments (TF1, etc.) are Numbered Consecutively Based on All Possible Cut Sites in the Molecule, Based on the Two Proteases Used to Digest the Sample

Proteolytic Frag. No.	AA sequence	Modification	% in Peak C	% in Peak D	% in Peak F
TF 22–27[a]	SAYFLHLTVKSDKPWFVAAMRPATAISADGPMNLLE	Oxidation	7.2	10.1	6.6
TF 32–34[b]	GRGVMWLNDR	Oxidation	2.4	2.4	2.7
TF 55	GIVYAGMGAGSVSVR	Oxidation	2.9	2.9	2.5
TF 67	ILLMLALTR	Oxidation	4.7	4.5	5.7
TF 62–66	TGNGIVPPDEELPGLVSDSLNPAHAR	Deamidation/ Succinimide	3.3	3.4	3.4

[a] The values given also include the oxidation of the homologous, less intense partial digest fragment ions TF23-27 AND TF26-27

[b] The values given also include oxidation of the partial digest fragment ion TF33-34

Peak D could be converted into Peak F after unfolding and refolding, but Peak F remained as Peak F post-denaturation. This suggested that Peak D may simply be an alternative conformer of Peak F, and that the differences between the IEX peaks were truly conformational in nature.

The peak isolate samples were therefore analysed using structural techniques. First, samples were examined using the low-resolution technique circular dichroism (CD) spectroscopy (data not shown). Using CD, it appeared that Peak C and Peak F were structurally similar, in contrast to Peak D particularly in the 210–225 nm region of the spectrum. Repeat analyses of Peak D indicated potentially significant differences in the spectra in the 210–225 nm trough region, but the reproducibility of the CD analyses was poor.

Due to the variability and lack of specificity in the CD data, orthogonal, higher-resolution structural techniques were employed. Samples of Peak isolates D and F were further analysed using small-angle X-ray scattering (SAXS) at beamline B21 at Diamond Light Source (Didcot, UK). SAXS is a sensitive technique for the analysis of the structure of macromolecules in solution. The D and F samples were sufficiently pure and monodisperse for SAXS measurement, with no evidence of protein aggregation observed, as evidenced by the linearity of the Guinier analysis of the data (see Supplementary Information). In Table VI, the radius-of-gyration (R_g) and scattering intensity at zero scattering vector ($q=0$) were approximated using Guinier analysis of the data (31, 32). The R_g values for the two peak isolates are

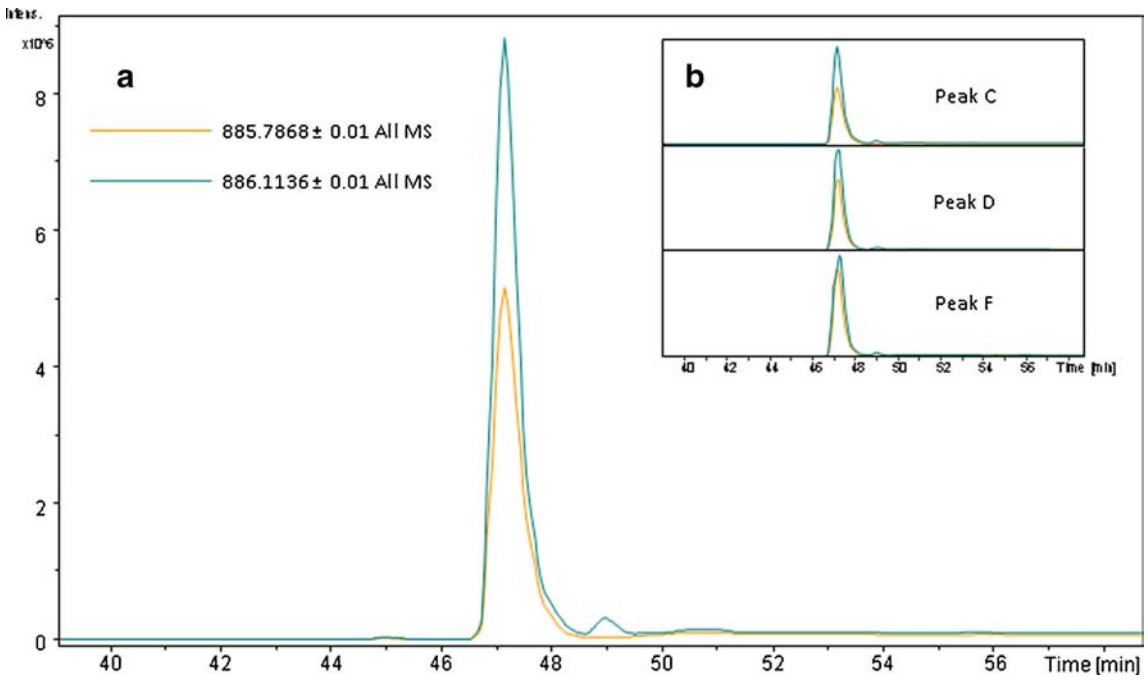

Fig. 5 LC-MS/MS results demonstrating low levels of deamidation present in all three IEX peaks. (**a**) An extracted ion chromatogram (EIC) of unmodified peptide TGNGIVPPDEELPGLVSDSLNPAHAR (885.7868 m/z) $[M+3H]^{3+}$ and deamidated peptide TGDGIVPPDEELPGLVSDSLNPAHAR (886.1136 m/z) $[M+3H]^{3+}$. There is a clear difference in retention time between the unmodified (ca 47 min) and deamidated peptide (ca. 49 min). (**b**) An overlay of EIC for modified and deamidated peptide for each of the isolated peaks(**c**,**d**,**f**). Levels of the deamidated peptide are consistent between the three IEX Peaks.

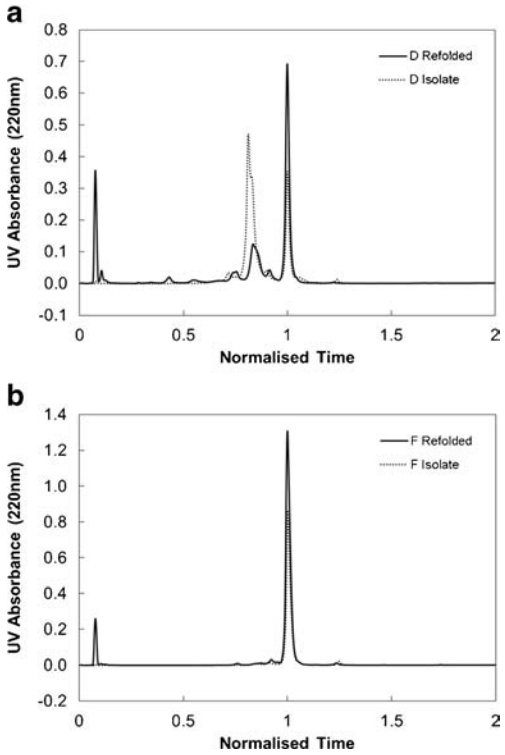

Fig. 6 Analytical IEX Chromatograms for IEX Peak Isolate Refolding Experiment. Peak isolates were exposed to strong denaturant (8 M urea plus added 2.2 M N-ethylurea) and dialysed back into 18.2 MΩ water before analysis by IEX. The IEX traces pre- and post- refolding are shown for Peak D (**a**) and Peak F (**b**).

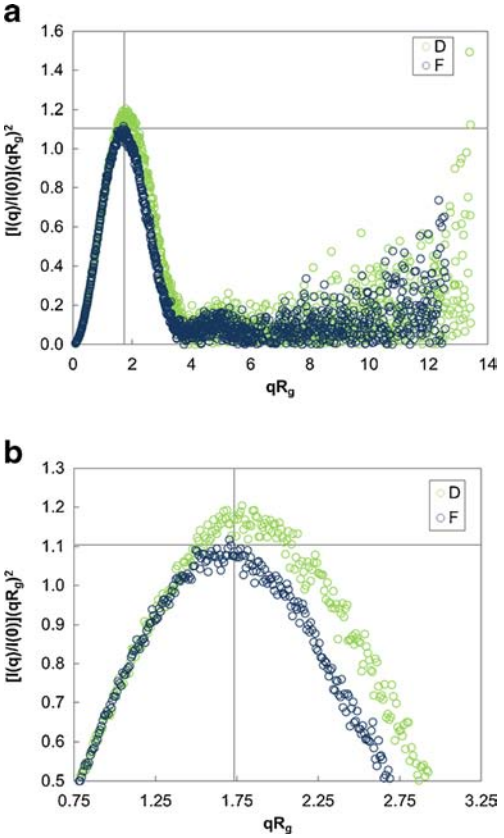

Fig. 7 Normalised Kratky Plots from Small-Angle X-ray Scattering Analysis of IEX Peak Isolates. The data are presented for analyses of 1.25 mg/mL enzyme samples in entirety (**a**) and as a close up to the area of interest (**b**). The cross hairs indicate the position of an ideal globular protein obeying Guinier's approximation. The nomenclature of the two axes is as follows: q, scattering vector; I(q), scattered intensity; R_g, radius of gyration; I(0), scattering at zero angle. The parameters R_g and I(0) were obtained from Guinier analyses of the collected SAXS data (not shown).

different with Peak D greater than Peak F, suggesting Peak D is less compact than Peak F.

These observed differences were also evident in the normalised SAXS Kratky plots (Fig. 7). The dimensionless or normalised Kratky plot (33) provides a semi-quantitative assessment of the state of the biomolecule in solution. For most compact, globular particles obeying Guinier's approximation, a peak maximum in the normalised Kratky plot should be observed at a qR_g (product of the scattering vector q and the radius of gyration) value of $\sqrt{3}$ with a magnitude of 1.104. This value is independent of particle size, composition and concentration, and is depicted by the cross-hairs in the normalised Kratky plots shown in Fig. 7. Deviations from this value indicate particle flexibility (34) or asymmetry (35). The maximum for peak isolate F was observed to agree with the theoretical Guinier prediction, indicating a perfectly globular protein. However, the Kratky maximum for peak isolate D was slightly shifted away from that of peak isolate F, indicating that peak D may not be perfectly globular. It is likely that D simply has a different surface-to-volume ratio compared with F.

Table VI Parameters Calculated from Guinier and Porod-Debye Analyses of Small-Angle X-ray Scattering Data for IEX Isolates of Peaks D and F

Sample name	Radius of gyration, R_g (Å)	Porod particle volume (Å^3)	Porod exponent	V_c (Å^3)	Molecular mass (kDa)
Peak D	32.9	192742	3.9	712.6	127
Peak F	31.6	181675	4.0	683.8	121

The idea that peak isolate D may simply have a larger surface-to-volume ratio was explored by using Porod-Debye analysis (not shown, a plot of q^4 *versus* q^4 times the scattering intensity, I(q)). Porod-Debye plots may be used to determine the particle volume as well as the Porod exponent, a guide to the overall particle shape. A Porod exponent of 4.0 indicates a perfectly globular protein. The results for peak isolates D and F (Table VI) show that D has a slightly larger particle volume compared with F, and that D has a Porod exponent slightly lower than the theoretical ideal of 4.0. The SAXS data can be further interrogated to calculate the volume of correlation, V_c, (Table VI) which is sensitive to conformational changes (36) and corroborates the differences between D and F in R_g. Taken together, these interrogations of the SAXS data strongly suggested that the main differences between the two IEX

peak isolates, D and F, were conformational in nature with Peak D occupying a comparatively less compact state than F.

SAXS data were also used to calculate the pair distance distribution function P(r). The P(r) distribution is a histogram of the set of electron–electron pair distances of the protein in solution. The P(r) distributions for peak isolate D and F samples were calculated and compared to the calculated P(r) function for the ErA crystal structure (Fig. 8) from the Protein Data Bank (PDB ID: 1O7J) (7). The P(r) curves for the Peak D and F isolates appear to compare well to each other. However, Peak F is shifted slightly towards smaller distances consistent with being more compact than D. Based on the resolution limit of the SAXS data used to calculate the P(r)-distributions, the two structures differ at a resolution of approximately 51Å. However, these differences are subtle indicating the solution structure is not in a different global arrangement compared with the crystal structure. Small differences observed for proteins by SAXS observed in the Kratky or P(r) treatments of the data have been shown to have significance (37–39). It is worth noting that the crystal structure 1O7J represents ErA without bound substrate and waters. For comparison purposes the ErA structure with bound L-glutamate (1HFW) was also used to calculate P(r) (data not shown) to investigate if any observed differences were due to substrate binding, but no effect of substrate binding on P(r) was found.

The peak isolates were also analysed using Ion Mobility Mass Spectrometry (IM-MS). To assess whether the two samples had different intact masses, a mass spectrum was obtained under denaturing conditions. No major differences in mass were observed between the two samples (Fig. 9). The experimentally determined mass was in very close agreement with the mass calculated from the protein sequence (Theoretical mass of 35054.09 Da). To probe any further differences between these samples, they were both analysed using native and IM-MS. Native mass spectrometry can be used to preserve non-covalent interactions within proteins and is one of the most accurate methodologies for obtaining the oligomeric state of proteins and protein complexes (40). IM-MS separates ions based on their size, charge and overall shape and can report on the conformational dynamics of the system under study (41). The native MS analysis revealed that both samples, D and F, existed as a tetramer in solution. There were no major differences in the mass between the two as calculated from the native MS spectra and no evidence of protein-protein aggregation from this analysis.

Ion mobility mass spectrometry (IM-MS) analysis, however, revealed a difference between the two samples. Sample D had a smaller collision cross section (CCS) compared to F (as calculated from the arrival time distribution peak tops shown in Fig. 9, panel c) indicating that D had an overall more compact conformation (Fig. 9). More significantly, however, the peak width of the CCS distribution for D was much broader than that of F (Fig. 9, panel c), indicating that D was sampling a wider range of conformations compared to F. Differences in the IM-MS full-width half-maximum of these peaks is indicative of increased conformational heterogeneity, as observed for other proteins (42, 43). These results strongly indicate that D has more conformational heterogeneity compared to F, an observation that fits well with the SAXS data and is probably the more relevant measure from the IM-MS experiments. At first glance, the observation that D had a more compact conformation compared with F based on CCS is contrary to the SAXS results described above. However, recently published results (44) demonstrated that

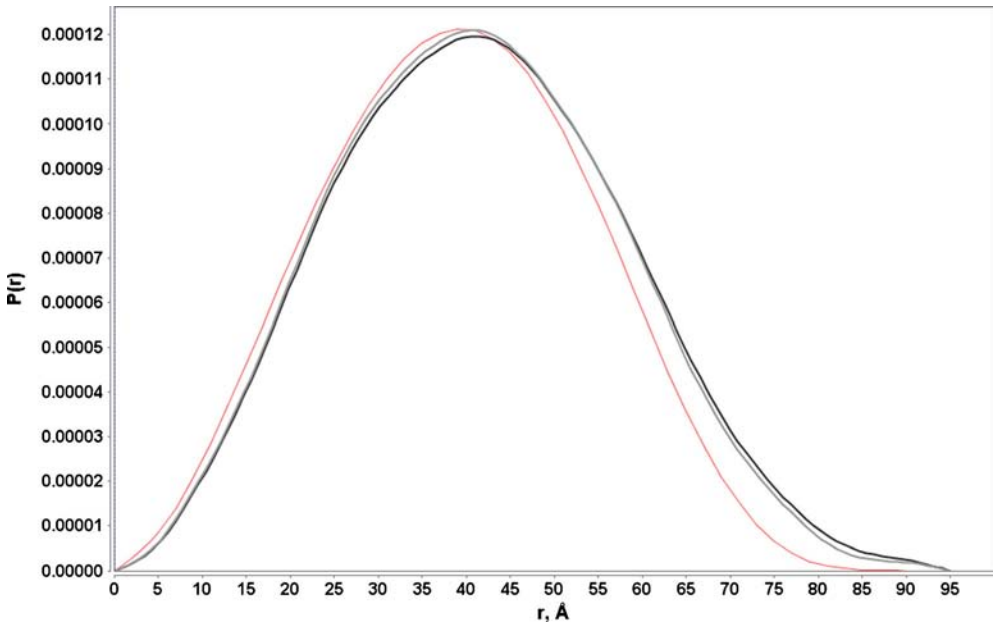

Fig. 8 Pair Distance Distribution Function, P(r). The SAXS derived P(r)-distribution gives a histogram of distances between all pairs of scattering electrons in the particle. The light grey curve represents the P(r) data for IEX Peak F and the dark grey, IEX Peak D. The red line represents the P(r) data calculated from the ErA crystal structure (PDB entry 1O7J).

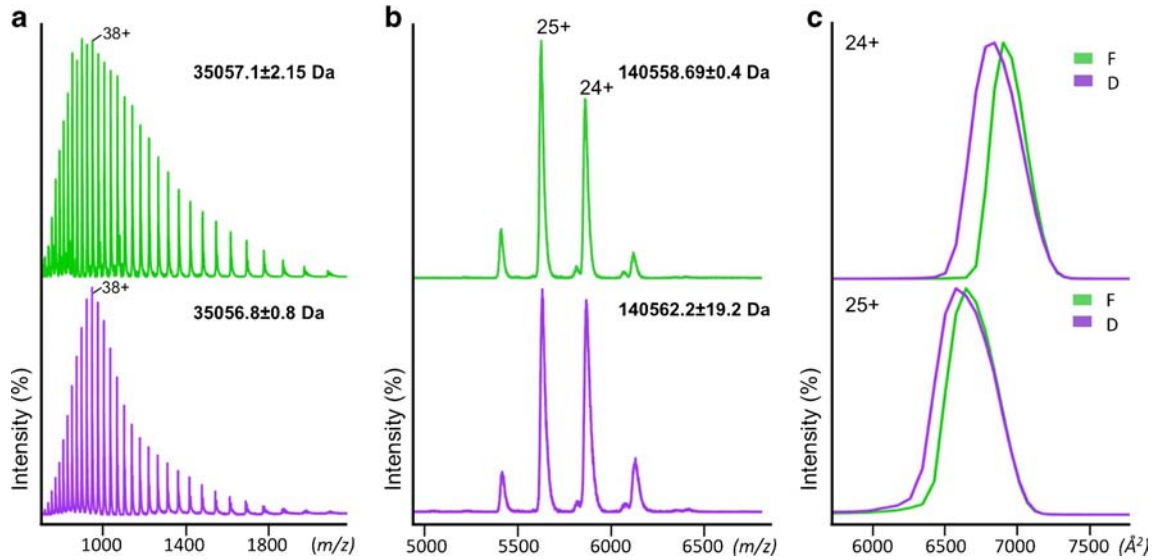

Fig. 9 Mass spectrometry analysis of ErA samples. (**a**) Denaturing mass spectra for F and D L-asparaginase samples coloured in green and purple respectively. (**b**) Native mass spectra of the F and D samples. In both cases the protein oligomeric states is that of a tetramer. (**c**) Overlay of the CCSs for the +24 and +25 charge states for F and D samples after quadrupole isolation.

there is a poor correlation between the square of R_g values and CCS measurements, a conclusion that is further supported by this work.

Slight conformational differences between the IEX peak isolates were measurable by multiple techniques. Based on these analyses, it appears that separation of ErA peaks during IEX analysis of ErA may be due to conformational changes in the enzyme. Both the IM-MS and the SAXS data suggest a different conformational state in Peak D compared with Peak F. In any case, the data suggest that for Peak D the observed conformational differences give rise to either increased exposure or shielding of certain residues to give an apparent decrease in p*I*, with early elution from the IEX column. Although the IEX peaks C and E were not evaluated using SAXS or IM-MS, peak D is the most prevalent in routine ErA samples (ca. 6–10% by peak area) compared with the other two peaks (ca. 3–5% for the sum of both). Therefore, peak D, which has been shown to be conformationally different to the main peak F, represents the bulk of the ErA modifications being measured by IEX.

The conditions that give rise to these conformational differences may occur during manufacture. The manufacturing process for ErA is complex and lengthy (9), with potential opportunities for generation of product variants. Furthermore, previous work had shown that ErA purified from *Erwinia* cells using affinity chromatography, and thus avoiding the standard manufacturing process, was virtually free of Peak D by IEX (data not shown), as was the recombinant WT ErA expressed in *E. coli* and also purified by affinity chromatography (25). Early research on ErA using fluorescence studies (45) indicated that exposure to high pH conditions caused a loosening of the enzyme structure. Similarly, CD studies of *E. coli* L-asparaginase (EcA), an enzyme with 46% identity (46) and high homology to ErA, indicated that exposure to pH levels greater than 10 degraded the secondary structure of the enzyme (47). The subunit interactions in the L-asparaginase tetramer (48) have been shown to be dominated by electrostatic interactions, which may be disrupted by local fluctuations in pH. Away from L-asparaginase, a similar situation was observed for the pheromone-binding protein (PBP) from the silkworm *Bombyx mori* (49). PBP was found to change conformation on exposure to certain pH conditions, and these conformational changes were observed by both IEX chromatography as well as CD.

CONCLUSIONS

The ion-exchange method routinely used for ErA product release measures acidic species (8–15%) that elute prior to the main peak. The most prominent of these acidic species has been shown to be a conformational variant as measured by multiple methods. This variant may be a consequence of the manipulations normally performed in the course of routine biopharmaceutical manufacture (and ErA in particular).

During biopharmaceutical development, ion-exchange HPLC is typically deployed to evaluate and measure the extent of primary-sequence modifications, such as deamidation, which are important to monitor from a regulatory perspective. It is perhaps easy to assume that acidic peaks resolved by ion-exchange are necessarily due to deamidation. This study on ErA ion-exchange peaks underscores the importance of gaining a holistic understanding of peaks resolved using ion-exchange analytical methods. The characterisation methods presented here should be considered during routine biopharmaceutical product development.

ACKNOWLEDGMENTS AND DISCLOSURES

The authors would like to thank Roger Hinton, Head of Development & Production for making facilities and funds available for this work, and Trevor Marks, Head of Process and Analytical Development Group, for facilitating these studies. Further thanks go to the entire Development & Production team at PHE Porton. MJD acknowledges support from the Biotechnology and Biological Sciences Research Council UK [BB/M012166/1]. NOL is funded by a BBSRC iCASE award BB/L015382/1.

REFERENCES

1. Duval M, Suciu S, Ferster A, Rialland X, Nelken B, Lutz P, *et al.* Comparison of *Escherichia coli*–asparaginase with *Erwinia*-asparaginase in the treatment of childhood lymphoid malignancies: results of a randomized European Organisation for Research and Treatment of Cancer—Children's Leukemia Group phase 3 trial. Blood. 2002;99(8):2734–9.
2. Beard MEJ, Crowther D, Galton DAG, Guyer RJ, Fairley GH, Kay HEM, *et al.* L-asparaginase in treatment of acute leukaemia and lymphosarcoma. Br Med J. 1970;1:191–5.
3. Pieters R, Hunger SP, Boos J, Rizzari C, Silverman L, Baruchel A, *et al.* L-Asparaginase treatment in acute lymphoblastic leukaemia: a focus on *Erwinia* asparaginase. Cancer. 2011;117(2):238–49.
4. Salzer WL, Asselin BL, Plourde PV, Corn T, Hunger SP. Development of asparaginase *Erwinia chrysanthemi* for the treatment of acute lymphoblastic leukemia. Ann N Y Acad Sci. 2014;1329: 81–92.
5. Wriston JC. Asparaginase. Methods Enzymol. 1985;113:608–18.
6. Aghaiypour K, Wlodawer A, Lubkowski J. Structural basis for the activity and substrate specificity of *Erwinia chrysanthemi* L-Asparaginase. Biochemistry. 2001;40:5655–64.
7. Lubkowski J, Dauter M, Aghaiypour K, Wlodawer A, Dauter Z. Atomic resolution structure of *Erwinia chrysanthemi* L-asparaginase. Acta Crystallogr D. 2003;59:84–92.
8. Miller M, Rao JKM, Wlodawer A, Gribskov MR. A left-handed crossover involved in amidohydrolase catalysis: crystal structure of *Erwinia chrysanthemi* L-asparaginase with bound L-aspartate. FEBS J. 1993;328(3):275–9.
9. Gervais D, Allison N, Jennings A, Jones S, Marks T. Validation of a thirty-year-old process for the manufacture of L-Asparaginase from *Erwinia chrysanthemi*. Bioprocess Biosyst Eng. 2013;36(4):453–60.
10. Jenkins N, Murphy L, Tyther R. Post-translational modifications of recombinant proteins: significance for biopharmaceuticals. Mol Biotechnol. 2008;39(2):113–8.
11. Wang W. Protein aggregation and its inhibition in biopharmaceutics. Int J Pharm. 2005;289(1–2):1–30.
12. Manning MC, Chou DK, Murphy BM, Payne RW, Katayama DS. Stability of protein pharmaceuticals: an update. Pharm Res. 2010;27(4):544–75.
13. Liu DT. Deamidation: a source of microheterogeneity in pharmaceutical proteins. Trends Biotechnol. 1992;10:364–9.
14. Weitzhandler M, Farnan D, Rohrer JS, Avdalovic N. Protein variant separations using cation exchange chromatography on grafted, polymeric stationary phases. Proteomics. 2001;1:179–85.
15. Zhao SS, Chen DDY. Applications of capillary electrophoresis in characterizing recombinant protein therapeutics. Electrophoresis. 2014;35(1):96–108.
16. Yang H, Zubarev RA. Mass spectrometric analysis of asparagine deamidation and aspartate isomerization in polypeptides. Electrophoresis. 2010;31(11):1764–72.
17. Hao P, Ren Y, Datta A, Tam JP, Sze SK. Evaluation of the effect of trypsin digestion buffers on artificial deamidation. J Proteome Res. 2015;14(2):1308–14. doi:10.1021/pr500903b.
18. Farnan D, Moreno GT. Multiproduct high-resolution monoclonal antibody charge variant separations by pH gradient ion-exchange chromatography. Anal Chem. 2009;81(21):8846–57.
19. Rea JC, Moreno GT, Lou Y, Farnan D. Validation of a pH gradient-based ion-exchange chromatography method for high-resolution monoclonal antibody charge variant separations. J Pharm Biomed Anal. 2011;54(2):317–23.
20. Han M, Guo A, Jochheim C, Zhang Y, Martinez T, Kodama P, *et al.* Analysis of glycosylated type II interleukin-1 receptor (IL-1R) by imaged capillary isoelectric focussing (i-cIEF). Chromatographia. 2007;66:969–76.
21. Sosic Z, Houde D, Blum A, Carlage T, Lyubarskaya Y. Application of imaging capillary IEF for characterisation and quantitative analysis of recombinant protein charge heterogeneity. Electrophoresis. 2008;29:4368–76.
22. Gandhi S, Ren D, Xiao G, Bondarenko P, Sloey C, Ricci MS, *et al.* Elucidation of degradants in acidic peak of cation exchange chromatography in an IgG1 monoclonal antibody formed on long-term storage in a liquid formulation. Pharm Res. 2012;29:209–24.
23. Khawli LA, Goswami S, Hutchinson R, Kwong ZW, Yang J, Wang X, *et al.* Charge variants in IgG1: isolation, characterisation, in vitro binding properties and pharmacokinetics in rats. MAbs. 2010;2(6): 613–24.
24. Gervais D, O'Donnell J, Sung M, Smith S. Control of process-induced asparaginyl deamidation during manufacture of *Erwinia chrysanthemi* L-asparaginase. Process Biochem. 2013;48(9):1311–6.
25. Gervais D, Foote N. Recombinant deamidated mutants of *Erwinia chrysanthemi* L-asparaginase have similar or increased activity compared to wild-type enzyme. Mol Biotechnol. 2014;56(10):865–77.
26. Gervais D, King D. Capillary isolelectric focussing of a difficult-to-denature tetrameric enzyme using alkylurea-urea mixtures. Anal Biochem. 2014;465:90–5.
27. Harms E, Wehner A, Jennings MP, Pugh KJ, Beacham IR, Röhm KH. Construction of expression systems for *Escherichia coli* asparaginase II and two-step purification of the recombinant enzyme from periplasmic extracts. Protein Expr Purif. 1991;2:144–50.
28. Derst C, Henseling J, Röhm KH. Probing the role of threonine and serine residues of *E coli* asparaginase II by site-specific mutagenesis. Protein Eng. 1992;5(8):785–9.
29. Pringle SD, Giles K, Wildgoose JL, Williams JP, Slade SE, Thalassinos K, *et al.* An investigation of the mobility separation of some peptide and protein ions using a new hybrid quadrupole/travelling wave IMS/oa-ToF instrument. Int J Mass Spectrom. 2007;261:1–12.
30. Sivalingam GN, Yan J, Sahota H, Thalassinos K. Amphitrite: a program for processing travelling wave ion mobility data. Int J Mass Spectrom. 2013;345:54–62.
31. Glatter O, Kratky O. Small-angle x-ray scattering. London: Academic; 1982. Chapter 28.
32. Feigin LA, Svergun DI. Structure analysis by small-angle x-ray and neutron scattering. New York: Plenum Press; 1987.
33. Rambo RP, Tainer JA. Characterising flexible and intrinsically unstructured biological macromolecules by SAS using the Porod-Debye law. Biopolymers. 2011;95(8):559–71.
34. Receveur-Brechot V, Durand D. How random are intrinsically disordered proteins? A small-angle scattering perspective. Curr Protein Pept Sci. 2012;13(1):55–75.

35. Durand D *et al.* NADPH oxidase activator p67(phox) behaves in solution as a multidomain protein with semi-flexible linkers. J Struct Biol. 2010;169(1):45–53.
36. Rambo RP, Tainer JA. Accurate assessment of mass, models and resolution by small-angle scattering. Nature. 2013;496:477–81.
37. Tian X, Langkilde AE, Thorolfsson M, Rasmussen HB, Vestergaard B. Small-angle x-ray scattering screening complements conventional biophysical analysis: comparative structural and biophysical analysis of monoclonal antibodies IgG1, IgG2, and IgG4. J Pharm Sci. 2014;103:1701–10. doi:10.1002/jps.23964.
38. Garst AD, Heroux A, Rambo RP, Batey RT. Crystal structure of the lysine riboswitch regulatory mRNA element. J Biol Chem. 2008;283(33):22347–51.
39. Guo W, West JM, Dutton AS, Tsuruta H, Kantrowitz ER. Trapping and structure determination of an intermediate in the allosteric transition of aspartate transcarbamoylase. Proc Natl Acad Sci U S A. 2012;109(20):7741–6.
40. Heck AJR. Native mass spectrometry: a bridge between interactomics and structural biology. Nat Methods. 2008;5:927–33.
41. Thalassinos K, Pandurangan AP, Xu M, Alber F, Topf M. Conformational States of macromolecular assemblies explored by integrative structure calculation. Structure. 2013;21:1500–8.
42. Zhou M, Morgner N, Barrera NP, Politis A, Isaacson SC, Matak-Vinkovic D, *et al.* Mass spectrometry of intact V-type ATPases reveals bound lipids and the effects of nucleotide binding. Science. 2011;334:380–5.
43. Hilton GR, Thalassinos K, Grabenauer M, Sanghera N, Slade SE, Wyttenbach T, *et al.* Structural analysis of prion proteins by means of drift cell and traveling wave ion mobility mass spectrometry. J Am Soc Mass Spectrom. 2010;21:845–54.
44. Marklund EG, Degiacomi MT, Robinson CV, Baldwin AJ, Benesch JLP. Collision cross sections for structural proteomics. Structure. 2015;23:791–9.
45. Homer RB, Allsopp SR. An investigation of the electronic and steric environments of tyrosyl residues in ribonuclease A and *Erwinia carotovora* L-asparaginase through fluorescence quenching by caesium, iodide and phosphate ions. Biochem Biophys Acta. 1976;434:297–310.
46. Minton NP, Bullman HMS, Scawen MD, Atkinson T, Gilbert HJ. Nucleotide sequence of the *Erwinia chrysanthemi* NCPPB 1066 L-asparaginase gene. Gene. 1986;46:25–35.
47. Illarionova NO, Petrov LN, Olennikova LV, Roshchin SN, Pasechnik VA, Haliapin BD, *et al.* Investigation of the L-asparaginase secondary structure in a wide pH region. Mol Biol Mosc. 1980;14:951–5.
48. Mezentsev YV, Molnar AA, Gnedenko OV, Krasotkina YV, Sokolov NN, Ivanov AS. Oligomerisation of L-asparaginase from *Erwinia carotovora*. Biochem Mosc Suppl Ser B Biomed Chem. 2007;1(1):58–67.
49. Wojtasek H, Leal WS. Conformational change in the pheromone-binding protein from *Bombyx mori* induced by pH and by interaction with membranes. J Biol Chem. 1999;274:30950–6.